DOI: 10.22226/2410-3535-2019-2-168-172 PACS: 61.80.–x; 02.70.Ns; 34.20.–b; 34.50.Bw; 36.40.–c

Molecular dynamics simulation of displacement cascades in B2 NiAl

N. T. H. Trung[1], H. S. M. Phuong[1,2], M. D. Starostenkov[1,†]

[1]Altai State Technical University, 46 Lenin St., Barnaul, 656038, Russia
[2]Nuclear Research Institute, 01 Nguyen Tu Luc St., Da Lat, 670000, Vietnam

[†]genphys@mail.ru

This study is focused on the behavior of B2 NiAl alloy under irradiation. For achieving this aim, we performed a series of molecular dynamics simulations of displacement cascades with the primary knock-on atom (PKA) energy from 1 keV to 40 keV. To ensure that the boundary effects were not important, the simulation boxes contained from 60×60×60 to 112×112×112 unit cells with 432 000 to 2 809 856 atoms, depending on the PKA energy. To correctly reproduce atomic interactions at short distances, the Mishin EAM potentials were stiffened in a short range using polynomial regression to join the equilibrium part of the EAM potential to a short range of ZBL potential and intermediate interatomic distance with the corresponding pairwise energy based on the density function theory calculation. To obtain statistically meaningful results, 10 simulations were performed for each PKA energy. Each cascade simulation lasted approximately from 12 ps to 42 ps, depending on the PKA energy; in these time intervals the number of Frenkel pairs (FP) became stable. We discuss in detail the time evolution of Frenkel pairs, the avalanche effect in the sonic phase and the origin of the permanent defect. The results from our simulations, including the number of stable Frenkel pairs, chemical composition, clustering of the defect production are in good agreement with the reports from the literature.

Keywords: molecular dynamics, displacement cascade, Frenkel pair, time evolution, amorphization, defect cluster.

УДК: 538.913

Молекулярно-динамическое моделирование каскадов атомных смещений в сплаве NiAl со сверхструктурой B2

Чунг Н. Ч. Х.[1], Фыонг Х. С. М.[1,2], Старостенков М. Д.[1,†]

[1]Алтайский государственный технический университет им. И. И. Ползунова, пр. Ленина, 46, Барнаул, 656038, Россия
[2]Институт ядерных исследований, ул. Нгуен Ты Лык, 01, Далат, 670000, Вьетнам

Исследование посвящено анализу поведения сплава NiAl со сверхструктурой B2 при облучении. Для достижения этой цели были проведены серии молекулярно-динамического моделирования каскадов смещений атомов в интервале энергии первично выбитого атома (ПВА) от 1 кэВ до 40 кэВ. Размеры моделируемых блоков кристаллов варьировались от 60×60×60 (432 000 атомов) до 112×112×112 (2 809 856 атомов) элементарных ячеек в зависимости от энергии ПВА. Для правильного воспроизведения атомных взаимодействий на малых расстояниях, потенциалы EAM Мишина были модифицированы на коротком расстоянии с помощью полиномиальной регрессии, чтобы соединить равновесную часть потенциала EAM с короткодействующей частью потенциала ZBL и промежуточного межатомного расстояния с соответствующей парной энергией согласно расчету с использованием теории функционала плотности. Для получения достоверных результатов для каждой энергии ПВА образца проводилось усреднение результатов по 10 расчетам. Физическое время моделирования составляло от 12 пс до 42 пс в зависимости от энергии ПВА, за это время число пар Френкеля оказывалось стабильным. Подробно обсуждается временная эволюция пар Френкеля, лавинный эффект в звуковой фазе и образование точечных дефектов. Результаты моделирования, включая число стабильных пар Френкеля, химический состав, кластеризацию и пространственное распределение дефектов, находятся в хорошем согласии с литературными данными.

Ключевые слова: молекулярная динамика, каскад атомных смещений, пара Френкеля, временная эволюция, аморфизация, кластер дефектов.

1. Introduction

Nickel-based alloys have excellent high temperature performance and corrosion resistance, and have been playing an important role in advanced nuclear energy systems, such as a molten salt reactor and a supercritical water reactor [1]. As a structural material in the nuclear energy systems, nickel-based alloys will be subjected to harsh work conditions, especially intensive radiation, which could be as high as a hundred dpa, and therefore the irradiation resistance of these alloys becomes one of the key performance for their application in nuclear systems of the new generation [2, 3, 4].

Among these Ni-base alloys, B2 NiAl (CsCl-type, space group Pm3m) is the most stable both at ambient and at very high pressure at room temperature [5]. The B2 NiAl compound is of particular interest from a mechanical point of view that motivates its extensive use in industry [6]. This class of intermetallic alloys is a very promising material for high temperature and pressure applications [7]. However, the behavior of B2 NiAl under irradiation is not an extensive study. The first cascade simulations in NiAl were performed more than 24 years ago in the works of Zhu et al. [8] and Doan et al. [9,10] with the PKA energy up to 12 keV, using EAM potentials. These potentials were joined by a spline to Ziegler-Biersack-Littmark (ZBL) potential with close atomic separation [11]. This is a well-known method to modify a potential for simulating the radiation damage, but this method has some drawbacks, since it neglects the impact of intermediate range repulsive interactions on the formation of cascade defects. Many reports from the literature show that stiffness at an intermediate distance has played an important role in the generation of primary damage [12,13,14,15,16].

In this paper, we presented the results of cascade simulations in B2 NiAl alloy at ambient temperature with the PKA energy from 1 keV to 40 keV using the Mishin EAM potential [17], which was modified in accordance with the procedure described in the work of Stoller et al. [18] that involves the use of *ab initio* calculations to determine the magnitude and spatial dependence of pair interactions at intermediate distances. The procedure to modify the Mishin potential for cascade simulation is beyond the scope of this paper, but it can be found in our other work [19]. The modified potential correctly reproduced not only the equilibrium lattice parameter, the cohesive energy, the lattice constant and other equilibrium properties, but also the threshold displacement energies of pure Ni, Al and their alloys B2 NiAl [19]. Therefore, it is suitable for simulating the radiation damage with a higher energy collision.

2. Method

The LAMMPS with GPU and Voronoi packages was used to simulate the displacement cascade in B2 NiAl with periodic boundary conditions applied in three directions [21,22,23]. In order to ensure that the boundary effects were not important, the simulation boxes contained from $60\times60\times60$ to $112\times112\times112$ unit cells with 432 000 to 2 809 856 atoms, depending on the PKA energy. The system was first equilibrated at 300 K in the canonical ensemble for 1 ns with a time step of 1 fs. After that, a random Ni PKA near the center of the simulation box was given kinetic energies of 1 keV, 5 keV, 10 keV, 20 keV, 30 keV and 40 keV along direction [135] to limit the channeling effect. Many publications have proved that the result calculated along direction [135] is representative of the average defect production for bcc metals and B2 ordered alloys [24]. The cascade simulations were performed in constant NVE with a variable time step in order to limit the distance traveled by atoms between the time step. All simulations were performed with a three layers wide Langevin bath at 300 K to dissipate energy induced by the PKA. This thermostat has a small effect on the outcome of the defect production, within our margin of error. We use Voronoi and Wigner Seitz cell analysis to determine the number of Frenkel pairs and OVITO (The Open Visualization Tool) for post-processing atomistic data obtained from the molecular dynamics simulation [25, 26]. The stochastic nature of primary damage events is an additional important consideration that requires a large number of primary knock-on atom collisions to be evaluated to achieve accurate statistics on computational simulations [27]. To obtain statistically meaningful results, 10 simulations were performed in each PKA energy. Each cascade simulation lasted approximately from 12 ps to 42 ps, depending on the PKA energy.

3. Results and discussion

3.1. FP time evolution

The dynamics of the FP is one of the most important characteristics of radiation damage. Using the terms suggested by Beland et al. [12], the FP time evolution can be divided into four phases: supersonic, transonic, sonic and thermal annealing.

Fig. 1 shows a typical time evolution of the number of FP during the displacement cascade. The supersonic phase begins immediately after the PKA has been given a kinetic energy. This atom moves through the lattice, encountering other atoms of the lattice. Such encounters may result in sufficient energy transfer to displace this atom of the lattice from its site, resulting in two displaced atoms. If this collision sequence continues, a series of tertiary knock-ons are produced, resulting in a collision cascade, and so on [28]. The number of defect production begins to increase as the PKA transfers its energy to other atoms in the lattice site. With the PKA energy range between 1– 40 keV, this phase lasted from 100 to 200 fs.

The results presented in Fig. 2 demonstrate that at the end of this phase the peak of the FP kinetic energy spectrum (the maximum kinetic energy per atom at a certain time during the simulation) decreases to only a few tens of eV nearby the value of its effective threshold displacement energy, which is equal to 40 eV in case of B2 NiAl. This figure has a stepped shape, because the kinetic energy of the cascade atoms, including the PKA, remain unchanged as they are able to travel through the lattice without direct collision with other atoms. When the collisions occur, the primary cascade atoms transfer a part of their energy to the secondary cascade atoms, and so on.

The supersonic phase is followed by the intermediate transonic phase, which is illustrated by a plateau on the FP time evolution curve. In this phase, the number of FP starts

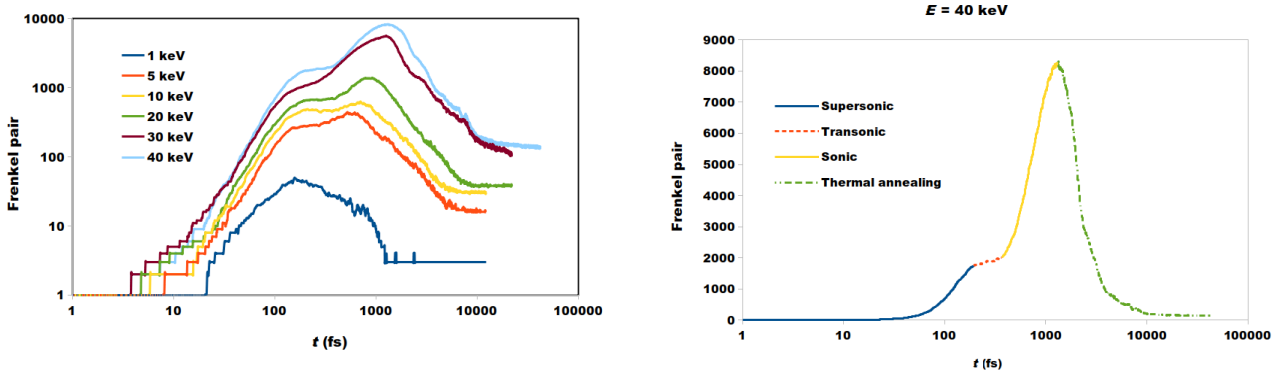

Fig. 1. (Color online) Frenkel pairs time evolution of displacement cascade from our simulation. The left panel is a log-log scale plot, while the right panel is a semi-log (linear-log) scale plot, which illustrates four phases of FP time evolution in displacement cascade with the PKA energy equal to 40 keV.

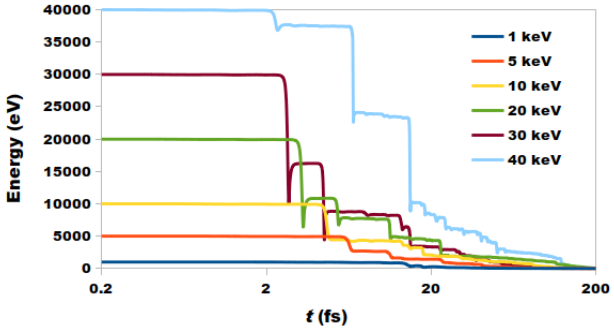

Fig. 2. (Color online) Semi-log scale plot of the maximum kinetic energy per atom at a certain time in the supersonic-transonic phase.

to increase slower, because the peak of the kinetic energy spectrum of displacement atoms has decreased below the value of the effective threshold displacement energy. The transonic phase can last up to 200 fs and is followed by the sonic phase.

The sonic phase is indicated by a sharp increase in the number of defect production, which leads to the FP peak that is in the range from 0.15 ps to 1.3 ps, depending on the PKA energy. As demonstrated in Fig. 1, the disorder zones expand dramatically and reach maximum at the FP peak. Many authors report that in this phase the disorder zone is locally melting, we have confirmed this statement using the radial distribution function. At the peak of FP, the kinetic energy of atoms in the disorder zone seems to follow the Maxwell-Boltzmann distribution with a mean local temperature around a few tens of thousands of Kelvin [20, 29]. Because of this, the disorder zone can be considered to be very hot, and therefore is called a heat spike or thermal spike [20, 29].

As we noticed earlier, in the transonic phase, the peak of the kinetic energy spectrum of the displacement atoms decreased below the value of the effective threshold displacement energy. From this point of view, a sharp increase of FP in the sonic phase might seem like a paradox. To understand the nature of this phenomenon, we will take a closer look at kinetic energy profile of the cascade atoms in this phase. At the end of the transonic, the energy of the PKA has transferred through the lattices in all direction. At the beginning of the sonic phase, the mean value (most probable value) of the energy in the kinetic energy spectrum of the atoms near the disorder zone has decreased to a few eV, which is comparable to the defect formation energy (i. e. vacancy and interstitial or FP formation energy). As a result, all atoms in the lattice around the disorder zone begin to vibrate with the same vibration energy close to the defect formation energy. Like the resonance phenomenon, these vibrations may stimulate the formation of a defect from atoms in vibrating lattices. This is followed by an avalanche of the defect production, which leads to the FP peak.

The thermal annealing phase begins after the peak of FP. After this the atoms do not have sufficient energy to create additional defects, and the recombination of closed space vacancies and interstitials becomes the dominant process. In our simulations, this phase lasts from 1 ps to 30 ps, at which point the number of FP in the system becomes stable (see video file in Supplementary Material).

3.2. Stable Frenkel pairs

A stable FP is a point defect, a survived interstitial, and a vacancy after the thermal annealing phase. This is related to permanent microstructural damage of the material under irradiation. The number of the survived FP is a widely used standard for estimating the primary damage of radiation in a material.

As mentioned above, cascade atoms with a kinetic energy larger or equal to the effective threshold displacement energy exist only in the supersonic and transonic phases. Therefore, the survived FP or permanent defects must be created during these phases. A recent work by Calder et al. also suggests that a stable FP is created during the supersonic and transonic phases by a destructive shockwave [12, 30]. By tracking the time profile and visual inspection of the stable FP in the simulation, we confirmed this statement. We analyzed the type of structure of a permanent defect by the common neighbor analysis method and found that an amorphous structure was formed in the defect zone. The dependence of the average stable Frenkel pairs on the PKA energy is shown in Fig. 3. In this energy range, the relationship is almost linear, like in the works of other authors [8,12, 31].

Compared to the Kinchin-Pease (KP) and Norgett-Robinson-Torrens (NRT) displacement model [32, 33], where the effective threshold displacement energy is chosen to be 40 eV, as recommended by SRIM (Stopping and Range of Ions in Matter) [11], our results, therefore, are only 35% of the NRT standard. These results are in good agreement

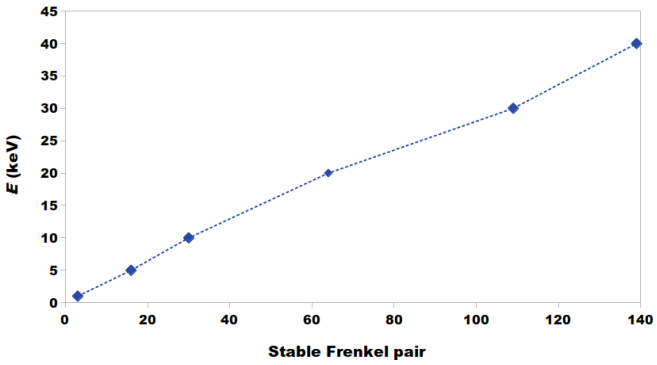

Fig. 3. The number of stable FP at the end of the thermal annealing phase as a function of PKA energy.

with the reports by other authors [9,27]. The actual defect production is sublinear with respect to the damage energy between ~0.1 and 10 keV, accounting for about 1/3 of the NRT-dpa prediction. At energies >10 keV, corresponding to the onset of the subcascade formation [27], the defect production increases linearly with the damage energy, but maintains the factor of ~3 lower than the NRT-dpa value [27,34]. In terms of damage production measuring, the NRT standard has several well-known problems. Since the NRT function is relatively simple, it severely overestimates the damage production in metals under the condition of the energetic displacement cascade [27]. In order to correct this shortcoming, a new analytical model, the so called "arc-dpa" (athermal corrected recombination), has been developed for the production of defects [27,34]. The results of our simulation are in perfect agreement with the prediction of this model with efficiency constant $\xi(E) \sim 2.85$.

3.3. Defect clustering

The formation of defect clusters in the displacement cascade has a strong influence on the evolution of the microstructure of the material. According to the work by Stoller et al. the formation of defect clusters is determined well before the onset of a thermal spike [35]. Fig. 4 shows the defect cluster distribution at the end of the thermal annealing phase with different PKA energy. Cluster size is defined as the number of defects in it.

As can be seen from Fig. 4, in-cascade clustering increases with increasing the PKA energy. Clusters with a size greater than 10 are observed only in displacement with the PKA energy exceeding 10 keV. The proportion of Ni in defect clusters is always higher than in the 50% NiAl alloy, from 55% to 72% of interstitial clusters is nickel, depending on the PKA energy. The higher the PKA energy, the higher the proportion of Ni in the survived interstitial clusters. This result is consistent with the aforementioned work made by Calder et al. [30], which describes the formation of a secondary shock wave in the transition region between the supersonic and transonic phases of the high energy cascade. If the PKA energy is smaller than 10 keV, then there are no collisions of the secondary shock wave, the cascade produces only isolated defects and small clusters by a supersonic destructive wave. In the high energy cascade displacement with the PKA energy exceeding 10 keV, when the secondary waves interfere, they create large interstitial clusters in the intersection volume [12,30]. In a number of recent works [36,37,38,39], the authors describe the formation of crowdion clusters moving at supersonic and subsonic speeds under irradiation. These crowdion clusters can be formed in 1D-crowdion (N-crowdions) or 2D (M×N-crowdions) or 3D (M×N×K-crowdions) and their dynamics could play an important role in the transfer of mass, energy and the formation of permanent defects in the crystalline solid under irradiation. In our simulation of the displacement cascade, we also observed the above-described phenomenon in the so-called "dynamic crowdions" as a result of the replacement collision sequences. This phenomenon will be discussed in more detail later in our next article.

4. Conclusion

We performed a comprehensive molecular dynamics study of the displacement cascade in B2 NiAl alloy. Both quantitative and qualitative methods were applied to study the time evolution, clustering properties, chemical composition and spatial distribution of the production of defects. A disordered amorphous structure was identified in the defect zone as a result of the radiation induced damage. We proposed possible qualitative explanations of the origin of the permanent defect and the avalanche effect in sonic

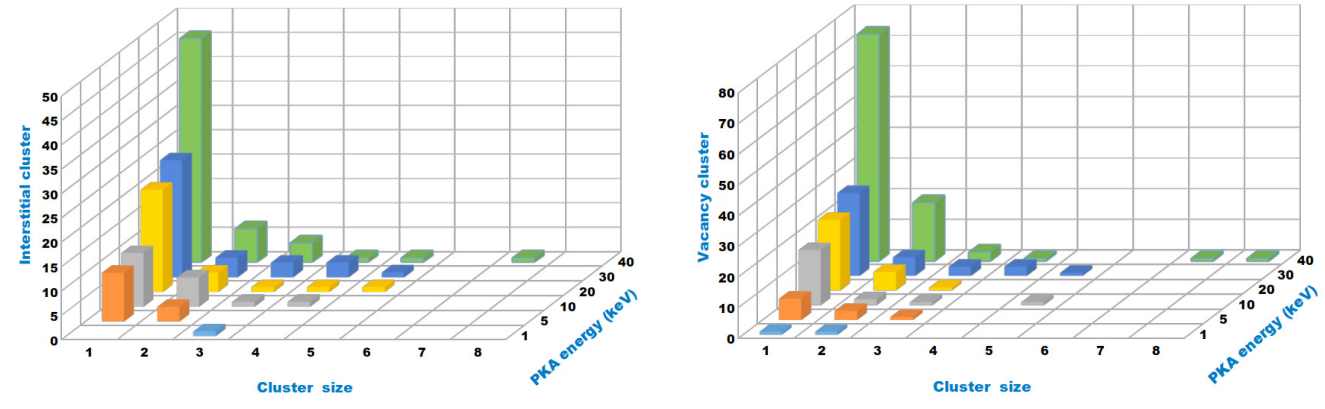

Fig. 4. (Color online) Defect cluster distribution as a function of PKA energy. For clarity, clusters with a size greater than 10 are not included in this figure.

phase of FP time evolution which leads to the peak of FP. Our work provides insight into understanding of the formation of a defect as a result of the radiation induced damage in the material in general and B2 NiAl alloy in particular.

Acknowledgments. This work was supported by the Russian Foundation for Basic Research and the Altai Krai (project №18-42-220002), and by the Ministry of Education and Science of Russian Federation (project № 3.4820.2017/БЧ).

Supplementary Material. *The online version of this paper contains supplementary material (video files demonstrating the time evolution of the Frenkel pairs in 30 keV displacement cascade simulation) available free of charge at the journal's Web site (www.lettersonmaterials.com)*

References

1. P. Yvon, F. J. Carré. Nucl. Mater. 385, 217 (2009) Crossref
2. T. Allen, J. Busby, M. Meyer. Mater. Today. 13, 14 (2010). Crossref
3. Development of Radiation Resistant Reactor Core Structural Materials, IAEA. https://www-legacy.iaea.org/About/Policy/GC/GC51/GC51InfDocuments/English/gc51inf-3-att7_en.pdf
4. P. Guo, J. M. Xue et al. Acta Metall. Sin. (Engl. Lett.). 28, 903 (2015). Crossref
5. W. Zhang et al. AIP Advances. 4, 057110 (2014). Crossref
6. A. Y. Lozovoi, Y. Mishin. Phys. Rev. B. 68, 184113 (2003), Crossref
7. R. Darolia, W. S. Walston, M. V. Nathal. Nasa Lewis Research Center. 561 (1996). Crossref
8. H. Zhu et al. Philosophical Magazine A. 71(4), 735 (1995). Crossref
9. N. V. Doan, R. Vascon. Radiation Effects and Defects in Solids. 141(1–4), 363 (1997). Crossref
10. N. V. Doan, H. Tietze. Nuclear Instruments and Methods in Physics. 102(1–4), 58 (1995). Crossref
11. J. F. Ziegler, J. P. Biersack and U. Littmark. The Stopping and Range of Ions in Matter. In: Bromley D.A. (eds) Treatise on Heavy-Ion Science. Springer, Boston, MA (1985). Crossref
12. L. K. Béland et al. J. Appl. Phys. 119, 085901 (2016). Crossref
13. C. S. Becquart et al. Phys. Rev. B. 66, 134104 (2002). Crossref
14. C. Becquart et al. J. Nucl. Mater. 280, 73 (2000). Crossref
15. D. Terentyev et al. J. Nucl. Mater. 351, 65 (2006). Crossref
16. C. Bjorkas and K. Nordlund. Nucl. Instrum. Methods Phys. Res. Sect. B. 259, 853 (2007). Crossref
17. G. P. P. Pun and Y. Mishin. Phil. Mag. 89, 3245 (2009). Crossref
18. R. E. Stoller et al. J. Chem. Theory Comput. 12 (6), 2871 (2016). Crossref
19. N. T. H. Trung et al. IOP Conf. Ser.: Mater. Sci. Eng. 447, 012004 (2018). Crossref
20. K. Nordlund, S. L. Dudarev. C. R. Physique. 9 (3 – 4), 343 (2008). Crossref
21. S. Plimpton. J. Comp. Phys. 117, 1 (1995). Crossref
22. W. M. Brown et al. Computer Physics Communications. 182 (4), 898 (2011). Crossref
23. C. H. Rycroft. Chaos. 19, 041111 (2009). Crossref
24. R. E. Stoller. Symposium R — Microstructural Processes in Irradiated Materials. 650, R3.5 (2000). Crossref
25. A. Stukowski. Modell. Simul. Mater. Sci. Eng. 20, 045021 (2012). Crossref
26. A. Stukowski. Modelling Simul. Mater. Sci. Eng. 18, 015012 (2010). Crossref
27. K. Nordlund et al. Journal of Nuclear Materials. 512, 450 (2018). Crossref
28. G. S. Was. Fundamentals of Radiation Materials Science: Metals and Alloys. Springer, Berlin (2007) 827 p. Crossref
29. T. Diaz de la Rubia et al. Phys. Rev. Lett. 60, 76 (1987). Crossref
30. A. Calder et al. Philos. Mag. 90, 863 (2010). Crossref
31. K. P. Zolnikov, A. V. Korchuganov and D. S. Kryzhevich. J. Phys.: Conf. Ser. 774, 012130 (2016). Crossref
32. G. H. Kinchin, R. S. Pease. Reports on Progress in Physics. 18(1), 1 (1955). Crossref
33. M. Norgett, M. Robinson and I. Torrens. Nucl. Eng. Des. 33, 50 (1975). Crossref
34. K. Nordlund et al. Report Nuclear Science. NEA/NSC/DOC (2015).
35. R. E. Stoller. Comprehensive Nuclear Materials. 1, 293 (2012). Crossref
36. E. A. Korznikova, I. A. Shepelev, A. P. Chetverikov, S. Y. Fomin, S. V. Dmitriev. IOP Conference Series: Materials Science and Engineering. 447, 012030 (2018). Crossref
37. S. V. Dmitriev, E. A. Korznikova, A. P. Chetverikov. Journal of Experimental and Theoretical Physics. 126, 347 (2018). Crossref
38. S. V. Dmitriev, N. N. Medvedev, A. P. Chetverikov, K. Zhou, M. G. Velarde. Physica Status Solidi — Rapid Research Letters. 11, 1700298 (2017). Crossref
39. A. P. Chetverikov, I. A. Shepelev, E. A. Korznikova, A. A. Kistanov, S. V. Dmitriev, M. G. Velarde. Computational Condensed Matter. 13, 59 (2017). Crossref